Tunable Coherent Radiation in the Soft X-Ray and Extreme Ultraviolet Spectral Regions

David T. Attwood, Patrick Naulleau, Kenneth A. Goldberg, Edita Tejnil, Chang Chang, Raul Beguiristain, Phillip Batson, Jeffrey Bokor, *Senior Member, IEEE,* Eric M. Gullikson, Masato Koike, Hector Medecki, and James H. Underwood

(Invited Paper)

***Abstract*— Undulator radiation, generated by relativistic electrons traversing a periodic magnet structure, can provide a continuously tunable source of very bright and partially coherent radiation in the extreme ultraviolet (EUV), soft X-ray (SXR), and X-ray regions of the electromagnetic spectrum. Typically, 1–10 W are radiated within a $1/N$ relative spectral bandwidth, where N is of order 100. Monochromators are frequently used to narrow the spectral bandwidth and increase the longitudinal coherence length, albeit with a more than proportionate loss of power. Pinhole spatial filtering is employed to provide spatially coherent radiation at a power level determined by the wavelength, electron beam, and undulator parameters. In this paper, experiments are described in which broadly tunable, spatially coherent power is generated at EUV and soft X-ray wavelengths extending from about 3 to 16 nm (80–430-eV photon energies). Spatially coherent power of order 10 μW is achieved in a relative spectral bandwidth of 9×10^{-4}, with 1.90-GeV electrons traversing an 8-cm period undulator of 55 periods. This radiation has been used in 13.4-nm interferometric tests that achieve an rms wavefront error (departure from sphericity) of $\lambda_{\rm euv}/330$. These techniques scale in a straightforward manner to shorter soft X-ray wavelengths using 4–5-cm period undulators at 1.90 GeV and to X-ray wavelengths of order 0.1 nm using higher energy (6–8 GeV) electron beams at other facilities.**

***Index Terms*— Coherent radiation, extreme ultraviolet, radiation, soft X-rays, undulator.**

I. Basic Properties of Undulator Radiation

THERE IS GREAT interest in the generation and application of short-wavelength coherent radiation. Shorter wavelengths extend the resolution limits of various microscopies, some of which require spatially and temporally coherent radiation [1]–[4]. At extreme ultraviolet (EUV), soft X-ray (SXR), and X-ray wavelengths, there are many atomic and molecular resonances that can be used for elemental and chemical identification. Undulator radiation is a special subset of synchrotron radiation generated when tightly confined, relativistic electrons traverse a long periodic magnet structure [5], [6]. In doing so, the electrons undergo near-sinusoidal oscillations, as shown in Fig. 1. Viewed in the frame of reference moving with the electrons [7], [8], power and angular distribution can be calculated as classical nonrelativistic dipole radiation at a wavelength $\lambda' = \lambda_u/\gamma$, where λ_u is the magnet structure period and

$$\gamma = 1\Big/\sqrt{1-\frac{v^2}{c^2}}. \tag{1}$$

Note that highly relativistic electrons of velocity v "see" a Lorentz contracted magnet structure of period λ_u/γ, and thus oscillate at a frequency

$$f' = c/\lambda' \tag{2}$$

in the frame of reference moving with the electrons. For a periodic magnet structure (undulator) of N periods, the electrons execute N cycles of oscillation and thus radiate a wave train of N periods, having a relative spectral bandwidth of $\Delta\lambda/\lambda \simeq 1/N$. Observed in the laboratory frame of reference, the dipole radiation is strongly Doppler shifted to

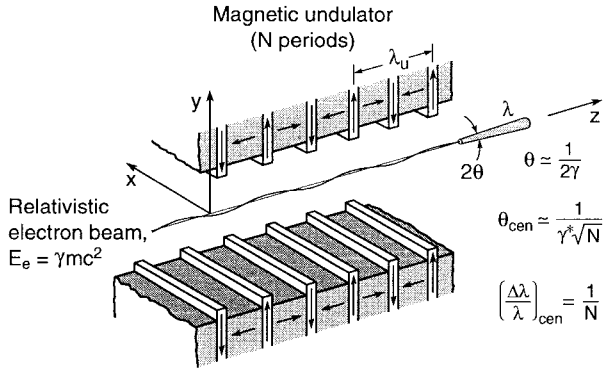

Fig. 1. Illustration of narrow-cone undulator radiation generated by relativistic electrons traversing a periodic magnet structure.

Manuscript received August 3, 1998; revised January 18, 1999. This work was supported in part by the Office of Basic Energy Sciences, Department of Energy, by DARPA's Advanced Lithography Program, by the Air Force Office of Scientific Research, by the Intel Corporation, and by the Extreme Ultraviolet Lithography Limited Liability Corporation.

D. T. Attwood, C. Chang, and J. Bokor are with the Center for X-ray Optics, Materials Sciences Division, Lawrence Berkeley National Laboratory, Berkeley, CA 94720 USA. They are also with the Department of Electrical Engineering and Computer Science, University of California, Berkeley, CA 94720 USA.

P. Naulleau, K. A. Goldberg, R. Beguiristain, P. Batson, E. M. Gullikson, H. Medecki, and J. H. Underwood are with the Center for X-ray Optics, Materials Sciences Division, Lawrence Berkeley National Laboratory, Berkeley, CA 94720 USA.

E. Tejnil is with Intel Corporation, Santa Clara, CA USA.

M. Koike is with the Japan Atomic Energy Research Institute, Kyoto, Japan.

Publisher Item Identifier S 0018-9197(99)03417-X.

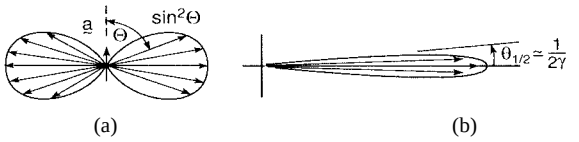

Fig. 2. (a) Illustration of the radiation pattern of an oscillating electron in the frame of reference moving at the average electron speed. (b) Illustration of the radiation pattern of a highly relativistic electron as observed in the laboratory frame of reference. The shortest wavelengths are observed on axis. (Following Hofmann [7]).

a frequency

$$f = \frac{f'}{\gamma(1-\beta\cos\theta)} = \frac{c}{\lambda_u(1-\beta\cos\theta)} \tag{3}$$

where $\beta = v/c$ and θ is the observation angle measured from the direction of motion. The $\sin^2\Theta'$ angular distribution of dipole radiation, where Θ' is measured between the directions of acceleration and observation in the frame of reference moving with the electrons, is dramatically transformed to a narrow forward cone, of half angle $\theta = 1/2\gamma$, in the laboratory frame of reference, by relativistic effects,[1] as illustrated in Fig. 2. This can be appreciated in terms of the angular transformations, for instance that

$$\tan\theta = \frac{\sin\theta'}{\gamma(\beta+\cos\theta')} \tag{4}$$

where θ' is measured from the same axis in the moving frame of reference. Physically, this is appreciated by observing that the angle-dependent relativistic Doppler shift preferentially moves energy to the forward direction: on-axis radiation is shifted to the shortest wavelengths, while off-axis radiation, having a wavevector component transverse to the motion, experiences a smaller Doppler shift, thus exhibiting a longer wavelength and lower photon energy in the laboratory frame of reference. For example, (4) shows that for β approaching unity and $\gamma \gg 1$, $\tan\theta$ is of order $1/\gamma$ for all θ'. At $\theta' = \pi/4$, where the dipole angular intensity is reduced to half its value on axis, $\theta = 0.4/\gamma$. Combining (1)–(3), using the small angle approximation for θ, noting that $\gamma^2 = 1/(1-\beta^2) \simeq 1/2(1-\beta)$, one finds that the Doppler-shifted frequency observed in the laboratory is

$$f = \frac{2c\gamma^2}{\lambda_u(1+\gamma^2\theta^2)} \tag{5}$$

or, in terms of wavelength,

$$\lambda = \frac{\lambda_u}{2\gamma^2}(1+\gamma^2\theta^2). \tag{6}$$

Thus, the on-axis wavelength is equal to the undulator period, λ_u, divided by $2\gamma^2$. For experiments described later in this paper, with $\lambda_u = 8.00$ cm and $\gamma = 3720$, the on-axis wavelength is decreased by the $1/2\gamma^2$ relativistic factor to about 3 nm, with longer wavelengths (off-axis) increasing rapidly for $\theta > 1/\gamma$. Note that the dipole radiation that appeared as a single wavelength in the frame of reference moving with the electron ($\lambda' = \lambda_u/\gamma$) with a relative spectral bandwidth $\Delta\lambda'/\lambda' = 1/N$ is spectrally broadened by the angle-dependent Doppler effects, as described by (6). This is illustrated in Fig. 3.

[1] With electron beam energy E_e in units of GeV, $\gamma = 1957\,E_e$ GeV, so that for $E_e = 1.90$ GeV, $\gamma = 3720$, and the nominal half-angle of synchrotron radiation ($\sim 1/2\gamma$) is 140 μrad.

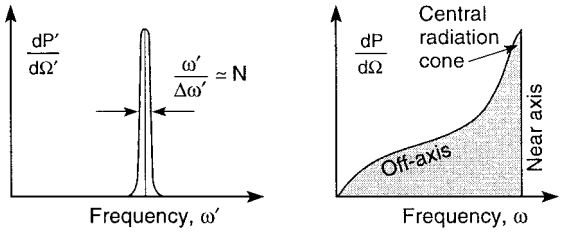

Fig. 3. (a) The radiation spectrum, as seen in the frame of reference moving with the electron, is narrow, with a relative spectral bandwidth of order $1/N$, where N is the number of oscillation periods. (b) In the laboratory frame of reference, the wavelengths are shorter, but the spectrum is broader due to off-axis Doppler effects. The region near the axis, containing a relative spectral bandwidth equal to $1/N$, is known as the "central radiation cone." (Following Hofmann [7].)

The preceding arguments are based on electrons traversing the magnet structure at a constant albeit relativistic velocity v. Of course, the electron experiences $\underset{\sim}{v} \times \underset{\sim}{B}$ forces as it moves through the magnet structure, causing it to oscillate and thus radiate. As energy, and thus velocity, is constant in a static magnetic field, the induced oscillations transverse to the direction of motion (z-direction) necessarily reduce the average axial velocity. This leads to a modified Lorentz contraction of the undulator period as seen by the electrons and a modified relativistic Doppler shift, through an effective value γ, which we will derive shortly. Motion of a relativistic electron in a periodic magnetic field is described by the rate of change of momentum due to the Lorentz force

$$\frac{d\,\underset{\sim}{p}}{dt} = -e\left(\underset{\sim}{E} + \underset{\sim}{v} \times \underset{\sim}{B}\right) \tag{7}$$

where $\underset{\sim}{p} = \gamma m\,\underset{\sim}{v}$, $\underset{\sim}{E}$, and $\underset{\sim}{B}$ are the electric and magnetic fields. In the undulator limit where radiated electric and magnetic fields are relatively weak,[2] the Lorentz force is dominated by the periodic magnetic field $B(z)$. Thus, for an initial velocity v_z in the z direction, and periodic magnetic field $\underset{\sim}{B}_y = B_o\cos(2\pi z/\lambda_u)\,\underset{\sim}{y}_o$ (see Fig. 1), the x component of the force equation is

$$m\gamma\frac{dv_x}{dt} = ev_zB_y$$

or

$$m\gamma\,dv_x = eB_o\cos(2\pi z/\lambda_u)\,dz$$

which integrates to

$$v_x = \frac{Kc}{\gamma}\sin(2\pi z/\lambda_u) \tag{8}$$

where

$$K = \frac{eB_o\lambda_u}{2\pi mc} \tag{9}$$

[2] This differs from the closely related case of a free-electron laser (FEL) where the radiated fields are strong enough to cause microbunching within the electron bunch, leading to enhanced radiated fields. To date, this has been achieved at longer wavelengths.

is a dimensionless parameter describing the periodic magnetic field [9]. Before considering acceleration and radiated power, we explore further the basic features of undulator radiation. One observation is that the electron makes an angle with respect to the z axis, which can be written, for the highly relativistic case ($\beta \to 1$, $v_z \lesssim c$), as

$$\tan\theta_e = \frac{v_x}{v_z} \simeq \frac{K}{\gamma}\sin(2\pi z/\lambda_u). \tag{10}$$

This corresponds to oscillations about the z axis, bounded by K/γ. As a consequence, K is often referred to as the magnetic deflection parameter. For $K \leq 1$, electron angular excursions lie within the natural emission cone of synchrotron radiation, and the resulting emission is referred to as undulator radiation. For the strong field case $K \gg 1$, one refers to wiggler radiation. The interplay between v_x and v_z can be understood in terms of the total velocity v and its relation to γ, where we recall that particle energy, and thus γ, is constant in a magnetic field. With $v^2 = v_x^2 + v_z^2$, the definition of γ becomes

$$\gamma = \frac{1}{\sqrt{1-\dfrac{v^2}{c^2}}} = \frac{1}{\sqrt{1-\dfrac{v_x^2}{c^2}-\dfrac{v_z^2}{c^2}}}$$

so that

$$\left(\frac{v_z}{c}\right)^2 = 1 - \frac{1}{\gamma^2} - \frac{v_x^2}{c^2}$$

or, to first order in the small parameter K/γ,

$$\frac{v_z}{c} = 1 - \frac{1}{2\gamma^2} - \frac{K^2}{2\gamma^2}\sin^2(2\pi z/\lambda_u).$$

This can be rewritten using the double angle formula as

$$\frac{v_z}{c} = 1 - \frac{\left(1+\dfrac{K^2}{2}\right)}{2\gamma^2} + \frac{K^2}{4\gamma^2}\cos(2k_u z) \tag{11}$$

where $k_u \equiv 2\pi/\lambda_u$. By averaging over a full cycle of the motion, we see that the average velocity in the z direction is decreased to

$$\frac{\overline{v}_z}{c} = 1 - \frac{\left(1+\dfrac{K^2}{2}\right)}{2\gamma^2}. \tag{12}$$

Comparing this to the case when K is zero, we can define an effective axial value

$$\gamma^* \equiv \frac{\gamma}{\sqrt{1+\dfrac{K^2}{2}}} \tag{13}$$

which can be used to better describe the Lorentz contraction and relativistic Doppler shifts considered earlier. Before proceeding to these corrections, we note that (11) contains a double-frequency axial motion term $\cos(2k_u z)$. Whereas v_x is proportional to K, as seen in (8), the double-frequency component of v_z is proportional to K^2. Indeed, this second harmonic ($n = 2$) motion leads to even higher harmonics through the z dependencies in the expressions for v_x and v_z [see (8) and (11)]. For small values of K, these harmonics are relatively weak, but for K exceeding unity they can become quite strong. This offers possibilities for achieving shorter wavelengths, albeit generally in a comb of harmonics with many radiating unwanted energy. Note that, in general, the even harmonics of motion are in the axial (z) direction and thus radiate angular patterns that are zero on-axis and that peak off-axis with a radial polarization [3], [7], [10]. The third harmonic ($n = 3$) has the same polarization as the fundamental ($n = 1$).

Accounting for the decreased axial velocity in the presence of a finite magnetic field B, corresponding to deflection parameter K as given in (9), the basic wavelength and frequency relations can be written as follows: with finite magnetic field and thus K-dependent axial velocity, the electrons experience, on average, a Lorentz contracted magnet period

$$\lambda' = \lambda_u/\gamma^*$$

and oscillate at a frequency

$$f' = c/\lambda' = c\gamma^*/\lambda_u$$

in the frame of reference moving with the electron's average velocity. As observed in the laboratory frame of reference, the radiation is Doppler shifted to frequencies (see (5) with $\gamma \to \gamma^*$)

$$f = \frac{2c\gamma^{*2}}{\lambda_u(1+\gamma^{*2}\theta^2)}$$

or, in terms of wavelengths,

$$\lambda = \frac{\lambda_u}{2\gamma^{*2}}(1+\gamma^{*2}\theta^2).$$

Substituting for γ^* from (13), one obtains the *undulator equation*

$$\lambda = \frac{\lambda_u}{2\gamma^2}\left(1+\frac{K^2}{2}+\gamma^2\theta^2\right) \tag{14}$$

which describes the radiated wavelengths as a function of angle and nondimensional magnet strength K in terms of the incident beam energy $\gamma = E_e/mc^2$. In principle, the undulator wavelength can be tuned by varying either γ or K. In practice, undulators are installed on large electron storage rings [11], [12] that simultaneously service many users of synchrotron radiation at fixed energy (γ). For this reason, wavelength tuning is achieved primarily by variations of K—achieved by opening and closing the magnet gap to decrease or increase the magnetic field strength [5], [6].

A convenient parameter for the study of undulator radiation is the "central radiation cone," defined as the range of angles θ, as observed in the laboratory frame of reference, that encloses a relative spectral bandwidth of $1/N$. The half-angle of this cone, θ_{cen}, can be determined from (14) by writing it twice, once for an axial wavelength λ_o at $\theta = 0$ and once for a shifted wavelength λ at the angle θ_{cen} such that $(\lambda - \lambda_o)/\lambda_o = 1/N$. Doing so, one obtains an expression for the half-angle of the central radiation cone

$$\theta_{\text{cen}} = \frac{1}{\gamma^*\sqrt{N}} = \frac{\sqrt{1+\dfrac{K^2}{2}}}{\gamma\sqrt{N}}. \tag{15}$$

For the undulator used in EUV experiments reported later in this paper, with $\lambda_u = 8.00$ cm, $\gamma = 3720$, $N = 55$, and K values from near zero to just over three, the "single electron" central cone half-angle varies from 36 to 85 μrad. Recall that $\theta_{\rm cen}$ contains a relative spectral bandwidth of $1/N$, approximately 2% in this case. According to (14), the range of wavelengths accessible on-axis ($\theta = 0$), with this variation in K, is approximately 3–16 nm, corresponding to photon energies extending from 80 to 430 eV. Third-harmonic radiation ($n = 3$), which is fairly strong for $K \geq 1$, generates radiation at one-third these wavelengths, or three times these photon energies, and thus can be used to extend operation of the 8-cm undulator to about 1 keV.

II. Undulator Power in the Central Radiation Cone

Power radiated in the central cone is most readily calculated in the frame of reference moving with the electrons [7], [8], where for small K the motion is nonrelativistic and the amplitude of oscillation is small compared to the radiated wavelength λ'. Thus, classical dipole radiation results are applicable in this frame of reference for low-K undulator radiation. To perform the calculation, one must know the acceleration $a_{x'}(t')$ in the moving frame of reference. To first order, it can be derived from the expression for velocity v_x in (8) by assuming that, for small K, $v_z \simeq zt$. This gives an expression for $v_x(t)$ that can be integrated to yield $x(t) = -(K/k_u\gamma)\cos\omega_u t$, where $\omega_u = k_u c$ and $k_u = 2\pi/\lambda_u$. Making the Lorentz transformation to the frame of reference moving at the average electron velocity $\overline{v}_z$, one obtains the equation of motion in the frame of reference moving with the electrons, and the acceleration

$$a_{x'}(t') = \frac{\gamma k_u c^2 K}{\left(1+\dfrac{K^2}{2}\right)}\cos\omega_u' t' \tag{16}$$

where

$$\omega_u' = \gamma^* \omega_u = \gamma k_u c\left(1+\frac{K^2}{2}\right)^{-(1/2)}$$

is the frequency of oscillation in the moving frame of reference. This can then be used in the classical dipole radiation formula for *power radiated per unit solid angle* by a single electron

$$\frac{dP'}{d\Omega'} = \frac{e^2 a'^2 \sin^2\Theta'}{16\pi^2\varepsilon_o c^3} \tag{17}$$

where a' is shorthand for the instantaneous electron acceleration given in (16) and Θ' is the observation angle measured from the direction of acceleration. For the consideration of power radiated only within the central radiation cone, the approximation $\sin^2\Theta' = 1$ incurs an error of only a few percent ($\sim 2/N$). Substituting (16) into (17), averaging over a full cycle of the motion, transforming back to the laboratory frame of reference, and multiplying by the solid angle of the central radiation cone $\Delta\Omega_{\rm cen} = \pi/(\gamma^*\sqrt{N})^2$, one obtains the average power radiated by a single electron into the central cone in the undulator limit ($K \leq 1$)

$$\overline{P}_{\rm cen}|_e = \frac{\pi e^2 c\gamma^2}{\varepsilon_o \lambda_u^2 N}\frac{K^2}{\left(1+\dfrac{K^2}{2}\right)^2}. \tag{18}$$

Assuming that the motion of electrons traversing the undulator is uncorrelated,[3] so that their intensities add rather than their fields, the power radiated can simply be multiplied by the number of electrons present. Expressing the result in terms of an average electron current, the time-averaged power radiated into the central radiation cone, as observed in the laboratory frame, is

$$\overline{P}_{\rm cen} = \frac{\pi e\gamma^2 I}{\varepsilon_o \lambda_u}\frac{K^2 f(K)}{\left(1+\dfrac{K^2}{2}\right)^2} \tag{19a}$$

which gives the power radiated at the fundamental ($n = 1$) wavelength, as given by the undulator equation (13), within a relative spectral bandwidth $\Delta\lambda/\lambda = 1/N$, which we used to define the central radiation cone. Note that, because the electron motion contributing to the fundamental motion lies completely in the x–z plane, the resultant radiation is horizontally polarized. Included in (19a) is a finite-K correction factor $f(K)$ that accounts for energy transfer [3], [13] to higher harmonics ($n > 1$), which becomes significant for $K > 1$. We have omitted consideration of harmonics in the brief outline of the theory above so as not to obscure an understanding of the basic features of undulator radiation. Some values of $f(K)$ are as follows: $f(0) = 1$, $f(0.5) = 0.94$, $f(1) = 0.83$, $f(1.5) = 0.73$, $f(2) = 0.65$, $f(2.5) = 0.61$, and $f(3) = 0.57$. In practical units, where the current is expressed in amperes and the undulator period in centimeters, (19a) becomes [13]

$$\overline{P}_{\rm cen}[{\rm W}] = (5.69\times 10^{-6})\frac{\gamma^2 I[{\rm A}]}{\lambda_u[{\rm cm}]}\frac{K^2 f(K)}{\left(1+\dfrac{K^2}{2}\right)^2} \tag{19b}$$

where again this is time-averaged power at the fundamental wavelength, in a spectral bandwidth $\Delta\lambda/\lambda = 1/N$, and within the central radiation cone. Fig. 4 shows a graph of predicted undulator power versus photon energy and K for an 8.00-cm, 55-period undulator at the advanced light source (ALS) in Berkeley [14], when operating with an electron energy of 1.90 GeV and an average current of 400 mA. We see that, within the nominal 2% relative spectral bandwidth, the 55-period undulator radiates between 0.5 and 1.5 W, tunable from about 80–430 eV (3–16 nm). Continuous tuning is achieved by variation of the magnetic gap (the separation between pole pieces), thus varying B_o, K, and λ, as described in (9) and (14). Due to the temporal duty cycle, 35-ps FWHM pulses every 2 ns, the peak power is about fifty times higher than the time-averaged power shown in Fig. 4. Results for other undulator periods and higher beam energies that extend capabilities to soft X-ray and X-ray wavelengths are easily

[3] This is the undulator limit of uncorrelated electron motion within the bunch. In the FEL limit, the electrons are partially bunched due to forces exerted by the radiated fields.

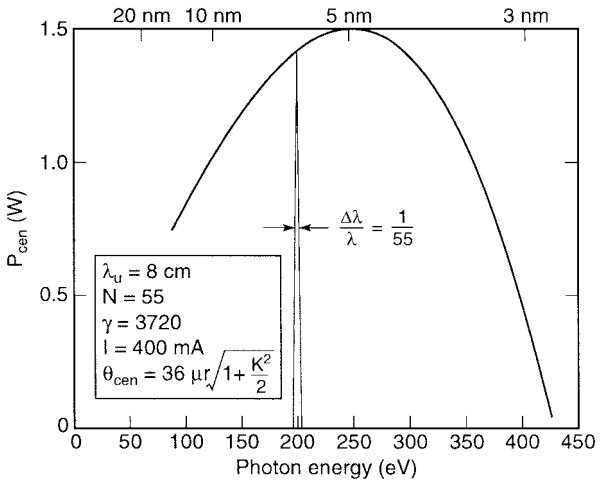

Fig. 4. Continuously tunable power in the central radiation cone of an 8.00-cm-period undulator at the ALS in Berkeley (1.90 GeV, 400 mA). The undulator has 55 magnet periods. The central radiation cone is characterized by a relative spectral bandwidth of 1/55, and a half-angle ranging from 36 to 85 μrad (at the longer wavelengths). Only radiation at the fundamental ($n = 1$) wavelength is included. Wavelength is shown across the top in nanometers.

obtained through use of (19). For example, the ALS also utilizes a 5-cm 89-period undulator, and the advanced photon source (APS) at Argonne National Laboratory in Illinois operates with a beam energy of 7 GeV ($\gamma = 13\,700$), a current of 100 mA, and utilizes a 3.30-cm, 72-period undulator to access wavelengths as short as 0.1 nm (12-keV photon energy) in the fundamental ($n = 1$).

Higher harmonics ($n > 1$) are a natural feature of undulator radiation. For low-K operation, the harmonics scale in power per unit solid angle approximately as n^4K^{2n}; thus, they rise rapidly as K approaches and exceeds unity. This subject is beyond the scope of this paper but is treated extensively in the literature [3], [7], [10]. As mentioned earlier, the 8-cm undulator at the ALS provides substantial third-harmonic ($n = 3$) radiation out to a photon energy of 1 keV, when operating at 1.90 GeV.

In principle, the central cone radiation for $n = 1$ lies within the angle $\theta_{\rm cen} = 1/\gamma^*\sqrt{N}$ given for a single electron in (15). However, the power described here in (19) is obtained by summing the contributions from many electrons, which have slightly different trajectories due to random motion within the beam. Generally, these angular variations are described in terms of a Gaussian angular distribution of rms deviation σ' from the z axis. As a consequence, the central radiation cone is increased. While not strictly correct, the resultant radiation cone half-angle is often expressed approximately as an addition in quadrature

$$\theta_T = \sqrt{\theta_{\rm cen}^2 + \sigma'^2}. \tag{20}$$

Generally, this is written separately for the orthogonal angular components σ'_x and σ'_y, as the electron beams are generally elliptical in nature. For the primary experimental results to be reported later in this paper, obtained at relatively long EUV wavelengths, σ'_x and σ'_y are considerably smaller than $\theta_{\rm cen}$. As noted earlier, for the 8.00-cm 55-period undulator, $\gamma = 3720$ and $K = 1$, $\theta_{\rm cen} = 44$ μrad, while for the ALS at this energy, $\sigma'_x = 23$ μrad and $\sigma'_y = 3.9$ μrad [15], so that θ_T is only slightly larger than $\theta_{\rm cen}$. This, however, is not always the case, particularly at X-ray wavelengths where the value of $\theta_{\rm cen}$ may be comparable to σ'. For situations where σ' is comparable to $\theta_{\rm cen}$, there is also an increase in the relative spectral bandwidth [13], [16] within that cone due to the increased role of off-axis Doppler-shifted radiation.

III. Spatially Coherent Undulator Radiation

We now turn our attention to the partially coherent nature [17], [18] of undulator radiation generated by a relativistic electron beam of relatively small beam size and divergence. In modern storage rings, so-called third-generation synchrotron radiation facilities [11], [12], the electron beams are typically elliptical in nature, with beam diameters of 50–500 μm and beam divergences of 10–40 μrad. Thus, a typical electron beam phase–space volume $d \cdot \theta$ is of the order of several nm $\cdot$ rad, comparable to that of diffraction-limited radiation in the EUV. Using pinhole spatial filtering techniques at EUV, soft X-ray, and X-ray wavelengths, it is possible to obtain a very high degree of spatial coherence at very useful power levels throughout this spectral region. Fig. 5 shows the basic technique in which a pinhole of diameter d is used in conjunction with an angular aperture θ, to selectively pass (filter) radiation within a phase–space product $d \cdot \theta$. In the limiting case where the intensity distribution is Gaussian in both spatial and angular distributions, with rms $(1/\sqrt{e})$ measures of diameter d and half-angle θ, the condition for full spatial coherence is given by [1], [13]

$$d \cdot \theta = \lambda/2\pi. \tag{21}$$

Thus, an ideal spatial filter, blocking radiation outside these limits, would transmit spatially coherent radiation having a power of

$$\overline{P}_{{\rm coh},\,N} = \left(\frac{\lambda/2\pi}{d_x\theta_x}\right)\left(\frac{\lambda/2\pi}{d_y\theta_y}\right)\overline{P}_{\rm cen} \tag{22}$$

where $d_x = 2\sigma_x$ is the horizontal "diameter" of the elliptical electron beam, $\theta_x = \sqrt{\theta_{\rm cen}^2 + \sigma_x'^2}$ is the divergence half-angle of radiation in the x–z plane, and $d_y = 2\sigma_y$ and θ_y are similar measures in the vertical plane. The orthogonal x–z and y–z spatial coherence filter factors are separated, as each has an independent maximum value of unity. The subscript $\mathrm{coh}N$ indicates that the transmitted power is spatially coherent and has an associated relative spectral bandwidth $\Delta\lambda/\lambda = 1/N$. In general, we can define as a measure of the longitudinal, or temporal, coherence length [17]

$$\ell_{\rm coh} = \frac{\lambda^2}{2\Delta\lambda} \tag{23}$$

so that without further monochromatization the central cone radiation has an associated coherence length $\ell_{\rm coh} = N\lambda/2$. The coherence length may be extended through the use of a monochromator, which narrows the transmitted spectrum at the cost of reduced power. For the ALS operating at 1.90 GeV, values of beam size and divergence in the undulators [15] are $d_x = 2\sigma_x = 520$ μm, $d_y = 2\sigma_y = 32$ μm, $\sigma'_x = 23$ μrad,

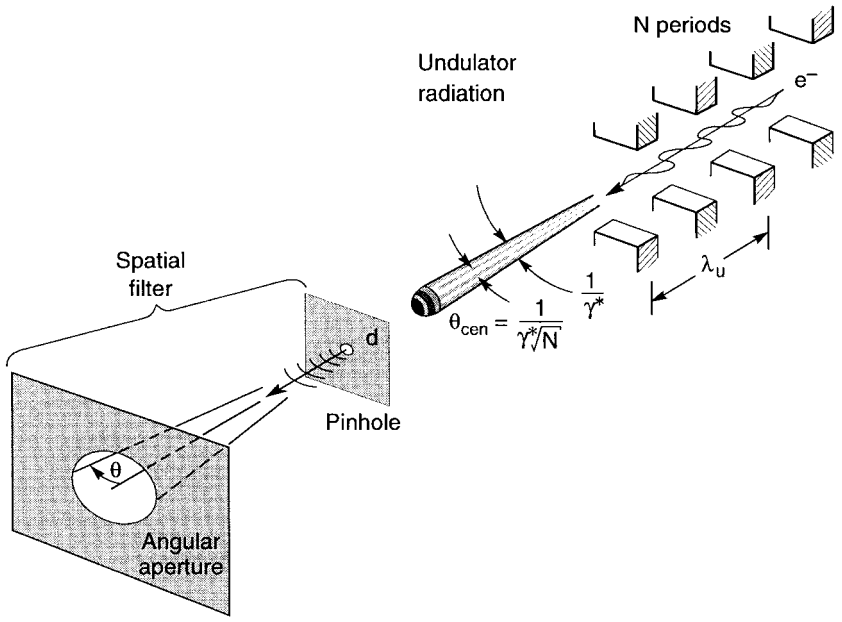

Fig. 5. Undulator radiation with a pinhole spatial filter.

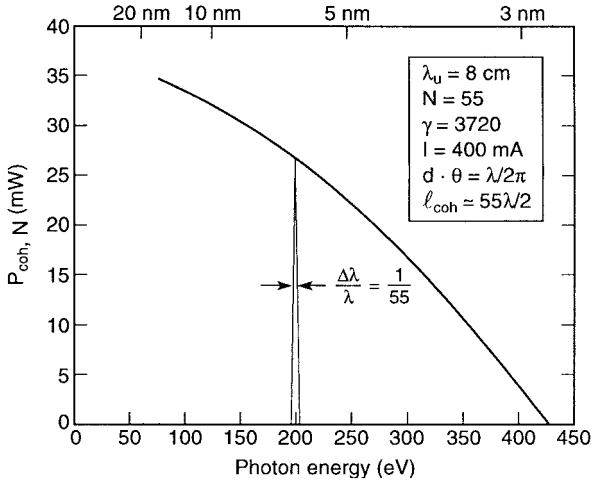

Fig. 6. Tunable spatially coherent undulator radiation is shown as a function of photon energy, within a relative spectral bandwidth of 1/55, as predicted for an 8.00-cm-period undulator at the ALS (1.90 GeV, 400 mA).

and $\sigma_y' = 3.9\ \mu$rad. Based on these parameters, and the use of (20) to estimate θ, the spatially coherent radiation (22) emitted from an 8-cm 55-period undulator is presented in Fig. 6 for a beam energy of 1.90 GeV and an average current of 400 mA. The radiation is continuously tunable through variation of the magnetic deflection parameter K, as given in (14). For these electron beam parameters, the spatially coherent power is predicted to decrease monotonically from about 35 mW at 80 eV to about 5 mW at 400 eV. In all cases, the relative spectral bandwidth is equal to about 2%. The corresponding longitudinal coherence length $\ell_{\rm coh} = N\lambda/2$ is about 360 nm at a wavelength of 13 nm. Tunable coherent power with these properties can be obtained with use of a simple pinhole and an angular aperture, as illustrated in Fig. 5. To reject spectral contamination due to higher harmonics, particularly for $K > 1$, a glancing-incidence mirror may be used.

In many applications, narrower spectral bandwidth or longer temporal coherence is required. This can be accomplished with a high-resolution monochromator, which can also be used to ensure high spectral purity, i.e., rejection of undulator harmonics. Typical applications involve the identification of atomic elements, including their chemical bonding, in scanning microscopy, and experiments such as interferometry or holography that require a certain coherence length. Fig. 7 shows a schematic diagram of the monochromator and optics [19]–[22] used on beamline 12.0 at the ALS to further monochromatize radiation from the 8-cm-period undulator. The beamline is primarily used for EUV interferometry [23]–[28] of multilayer-coated [29], [30] optical systems [31], [32] intended for use in EUV lithography (EUVL) applications [33], [34] at wavelengths from 11 to 14 nm [29], [30]. The monochromator provides a relative spectral bandwidth variable between 10^{-2} and 5×10^{-4}, at photon energies extending from about 60 to 250 eV. The latter is set by glancing incidence mirrors selected to suppress odd harmonics above the spectral region of interest for testing of EUVL optics. The range of spectral bandpass is set by the selection of a specific grating for use in the monochromator: several different gratings of different dispersion are available. In addition to providing narrow-band monochromatization, typically of order 1/1100 in normal operation, the beamline also projects a geometric 65 : 1 reduced image of the source at the entrance pinhole of the EUV intererometer. It is there that spatial filtering is used, in conjunction with the acceptance aperture of the EUV optical system under test. In fact, the pinhole often serves as the equivalent "exit-slit" of the monochromator. The monochromator is of constant-deviation type, employing a varied line-space plane grating [20] that corrects for aberrations of the monochromator while maintaining a fixed exit-slit position during wavelength tuning. Interchangeable gratings permit spectral bandwidth and coherence length to be traded off with available photon flux.

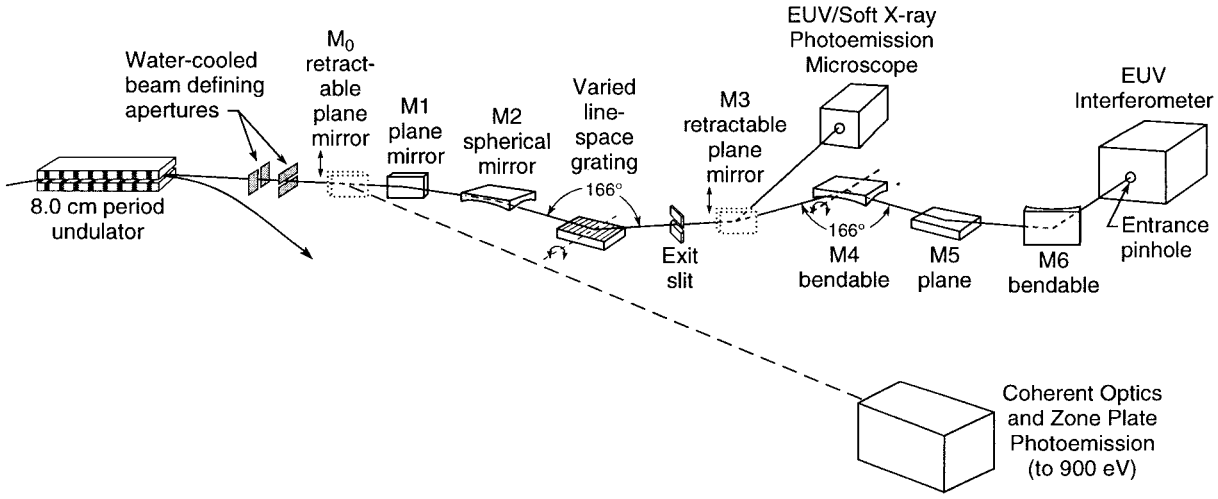

Fig. 7. A coherent optics beamline used for spatial and spectral filtering of undulator radiation. The grating and exit slits provide spectral filtering, typically to $\lambda/\Delta\lambda = 1100$. The reflective optics (mirrors) refocus the source at a 65:1 demagnification on an entrance pinhole at each station. The angle of incidence of these mirrors is chosen to cut off radiation above 250 eV. The pinhole diameter is selected to provide spatial filtering for the given incident radiation cone and/or the acceptance cone within each experimental chamber. Two separate branch-lines are available as shown and are selected by a retractable mirror. A third branchline (dashed line) would extend operation to 400 eV in the fundamental ($n = 1$), and to about 1 keV using third-harmonic radiation ($n = 3$) and beamline mirrors of smaller glancing incidence angle.

Use of a monochromator and beamline optics introduces a significant loss of power. There is both a fixed "insertion loss" due to the finite mirror reflectivities and a grating loss due to the nonunity diffraction efficiency to the desired order. Taking the latter as 30%, and utilizing five glancing incidence mirrors each having 80% reflectivity, gives an overall beamline efficiency factor η of about 10%. In addition, considering that the beamline accepts only central cone radiation of relative spectral bandwidth $1/N$, and then filters it to a smaller value $\Delta\lambda/\lambda$, there is an additional loss of flux equal to $(\Delta\lambda/\lambda)\ N$. For $N = 55$ and a monochromator bandpass set for nominal operation at $\Delta\lambda/\lambda = 1/1100$, this bandpass narrowing reduces transmitted power by an additional factor of 0.05. Consequently, as used in these experiments, available coherent power within the narrowed spectral bandpass will be reduced by a factor $\eta N(\Delta\lambda/\lambda) = 5 \times 10^{-3}$. Fig. 8 shows a curve of projected coherent power, again following (19) and (22), but now accounting for the narrowed relative spectral bandwidth of 1/1100 and a beamline efficiency of $\eta = 10\%$.

To utilize these levels of coherent power in experiments, one must spatially filter the undulator radiation. In the process of spatial filtering, the initial photon beam phase–space product $d \cdot \theta$ is too large and must be reduced through constraints on either d or θ, or both. For the experiments reported here, the choice was driven by the numerical aperture (NA) and demagnification of the first optical system under test, a $10\times$ Schwarzschild system of NA $= 0.08$, with multilayer coatings for use at 13.4-nm wavelength. As the optics were to be tested by illumination from the small-NA side, this required an optical acceptance half-angle of 8 mrad. With a nominal central cone half-angle of just under 80 μrad, and an angular magnification of 65, the beamline optics provide an illumination cone of about 5.2 mrad, purposely chosen to be somewhat smaller than the test optic NA. The choice of an intentionally small pinhole increases the illumination

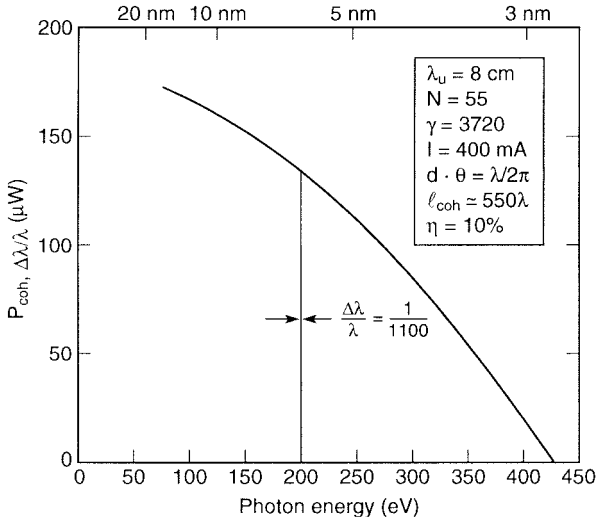

Fig. 8. Tunable spatially coherent undulator radiation as a function of photon energy, for a relative spectral bandwidth of 9×10^{-4}, and a longitudinal coherence length of 550λ. Curves are for an 8.00-cm-period undulator at the ALS operating at 1.90 GeV, assuming a monochromator/beamline efficiency (insertion loss) of $\eta = 10\%$, in addition to reduced flux associated with the narrowed spectral bandpass.

angle, through diffraction, as desired. The pinhole size d was chosen to give an Airy pattern null equal to twice the acceptance half-angle of the optic, or about 16 mrad. For an Airy pattern, the first angular null [17] is at $\theta_{\text{null}} = 1.22\lambda/d$. For $\theta = 16$ mrad and $\lambda = 13.4$ nm, which corresponds to a pinhole diameter of 1.0 μm, the size nominally used. The relatively small pinhole size provides improved spatial coherence across the fixed numerical aperture. Furthermore, by using only the central portion of the Airy pattern, improved illumination uniformity and wavefront quality are obtained. These benefits come at the cost of a reduction in available coherent power.

IV. Computational Modeling with a Sharply Defined Emission Cone

The formulation of spatially coherent power as given in (22) is a convenient model, generally very useful at soft X-ray and X-ray wavelengths were $\theta_{\rm cen}$ is smaller (higher γ, larger N), and is comparable to σ', such that the angular distribution of central cone radiation is smoothed to a near-Gaussian distribution. However, the model is not an accurate predictor for non-Gaussian intensity distributions. For example, it has the potential to underestimate coherent power in the case where $\theta_{\rm cen} \gg \sigma'_{x,y}$. In this case, the phase–space photon density within $d \cdot \theta$ is higher than implied by the Gaussian model, and thus higher spatially coherent power is available. Furthermore, the angular emission associated with the central cone may be quite sharp, producing an Airy-like intensity pattern in the far field. Here we present a computational model that is more representative of our undulator beamline. In the limit of a sharply defined angular radiation pattern (set by the sharp monochromator bandpass), this results in a coherent power 2.8 times higher that than given by a Gaussian distribution, in each direction. Thus, if both $\sigma'_x/\theta_{\rm cen}$ and $\sigma'_y/\theta_{\rm cen} \ll 1$, the resultant coherent power can be 7.7 times higher than a larger phase–space Gaussian distribution. For the EUV experiments at 13.4 nm considered here, $K = 2.64$ such that with $\theta_{\rm cen} = 77$ μrad, $\sigma'_x = 23$ μrad, and $\sigma'_y = 3.9$ μrad, the sharp angular model is good in the vertical (y) direction, and fairly good in the horizontal (x) direction. We thus consider radiation with a sharply defined emission cone of half-angle $\theta = 80$ μm, obtained using (20) with $\theta_{\rm cen} = 77$ μrad at 13.4 nm, and the σ' values given above.

The beamline monochromator plays a major role in defining this sharp angular emission through its bandpass capability. Furthermore, the beamline optics magnify this angle by 65, while decreasing the image size. As seen in the pinhole plane, the emission arrives with an equivalent focusing numerical aperture of NA $= 65$ (80 μrad) $= 5.2$ mrad. It would then focus a point source to an Airy pattern with a first null diameter [16] $d_{\rm null} = 1.22\lambda/{\rm NA} \simeq 3.1$ μm. We might, in fact, use a pinhole of this diameter to define the coherent power passed by the spatial filter. As pointed out above, however, we purposely use an undersized 1-μm-diameter pinhole to overilluminate the optic under test, thus providing improved intensity uniformity and coherence. Fig. 9 shows two numerical simulations of our experiment, both based on the assumption that monochromatization leads to a sharply defined angular emission cone of NA $= 5.2$ mrad, as seen at the pinhole plane. In Fig. 9(a), a numerical simulation shows that the projected image of the Gaussian beam of (2σ) size 520 μm $\times$ 32 μm would be imaged to the pinhole plane by an ideal 65 : 1 reduction lens of 5.2 mrad NA. The image is 9.4 μm $\times$ 1.4 μm FWHM, set largely by the wavelength and NA in the vertical direction ($d_{\rm FWHM} = d_{\rm null}/2.36 = 1.3$ μm, increased slightly by the projected vertical source size $1.18 \cdot 2\sigma_y/65 = 0.6$ μm FWHM). The horizontal size is set largely by the relatively large horizontal beam size, $2\sigma_x/65$, with a 1.18 multiplier to convert from $1/\sqrt{e}$ to FWHM. Based on the assumption of a sharply defined angular distribution of radiation, these computations predict a transmitted power of 959 μW through a diffraction-limited 3.1-μm-diameter pinhole, and 148 μW through a smaller 1.0-μm-diameter pinhole.

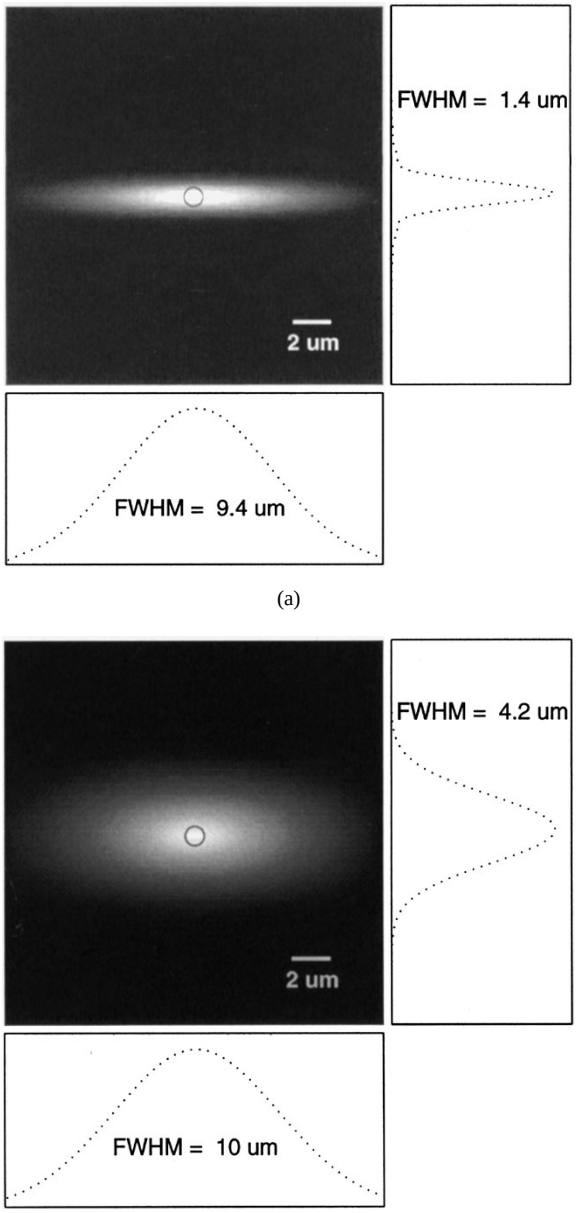

Fig. 9. (a) Numerical simulation of the 13.4-nm wavelength undulator radiation imaged to the pinhole plane assuming an ideal 65 : 1 reduction optical system of 5.2 mrad NA, based on the assumption of a sharply defined emission cone. The pinhole shown has a 1-μm diameter. (b) Numerical simulation of 13.4-nm intensity distribution in the pinhole plane, as in (a), now including an aberrated point spread function, represented by a circularly symmetric Gaussian of 4-μm FWHM in the pinhole plane. The aberration is chosen to simulate focusing errors by the final KB optics in these experiments. Again, a 1-μm-diameter pinhole is shown.

Fig. 9(b) shows a calculation of the projected source image accounting for aberrations in the final KB focusing optics (mirrors M4 and M6 in Fig. 7). The point spread function of the aberrated KB is modeled here as a circularly symmetric Gaussian with a FWHM of 4 μm in the pinhole plane. The

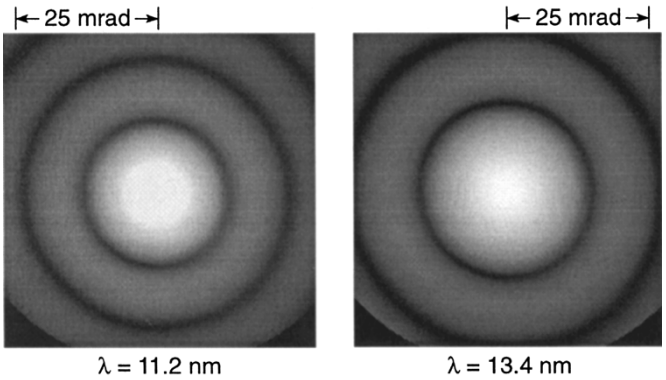

Fig. 10. Measured Airy patterns obtained by pinhole spatial filtering of undulator radiation, at wavelengths of 11.2 and 13.4 nm. The pinhole-to-CCD distance is 410 mm and the image sizes are 23 × 23 mm. The data was obtained using beamline 12.0 at the ALS in Berkeley.

resultant projected image is 10 μm × 4.2 μm FWHM, similar to the 9.4 μm × 4 μm FWHM we observe experimentally. Inclusion of the effect of aberrations in the KB focusing optics reduces the calculated power transmitted by a 3.1-μm-diameter pinhole to 554 mW, and that of a 1.0-μm-diameter pinhole to 62 μW.

V. Experimental Results

Experiments have been conducted utilizing narrow-band spatially coherent radiation from the 8-cm 55-period undulator at the ALS. Fig. 10 shows Airy patterns obtained at wavelengths of 11.2 and 13.4 nm, with a 1.1-μm-diameter pinhole. In each case, the relative spectral bandwidth is about 9×10^{-4}. The images were recorded on a back-thinned EUV CCD camera at a distance of 410 mm from the pinhole. The image size is 22 × 22 mm (NA = 27 mrad). Power in the Airy pattern, normalized to a 1-μm pinhole, was measured to be 9.4 μW for the 13.4-nm wavelength. To compare this with predicted values, we note that, at 13.4 nm (92.5 eV), Fig. 8 predicts a spatially coherent power (based on a Gaussian angular distribution and a 1/1100 spectral bandwidth) of about 167 μW. The difference is a factor of about 18. Two factors largely explain the difference. First, the pinhole at 1-μm diameter is undersized, purposely chosen to trade power for improved wavefront sphericity and uniformity of intensity in subsequent interferometric testing of EUV optical systems. Second, there is a loss of about a factor of three due to aberrations in the KB optics (4.2 μm/1.4 μm). Hence, in the present experiments, we have a reduction in coherent power by a factor of 0.15 due to the undersized pinhole, and by about 0.33 due to aberrations in the KB optics, for an overall reduction factor of about 20. Yet, as described above, this simplified model is expected to underestimate the coherent power available to the experiment. The simulation based on a sharply defined angular emission cone, as presented in Fig. 9(b), predicts a coherent power transmitted by the 1-μm-diameter pinhole of 62 μW, about 6.6 times the measured value, even after accounting for the reduced pinhole size and aberrations in the KB system. We believe this modeling, while not perfect, to be a better predictor than the Gaussian model for the parameters of interest here. Sources of this discrepancy include a possible overestimate of coherent power associated with the assumed sharpness of the angular distribution of undulator radiation and carbon contamination of beamline optics that has been observed and does reduce beamline efficiency. Furthermore, the estimate is expected to improve as we obtain better measurements of the beamline parameters σ and σ'. Despite these differences in modeling, the measured values indicate very useful levels of average coherent power for experiments involving undulator radiation at modern synchrotron facilities like the ALS.

An important question of interest in the application of spatially coherent radiation is the deviation of the wavefront from a sphere. This has been examined interferometrically, as described in Fig. 11. The interferometer has been developed as part of a program to characterize multilayer coated optical systems for EUVL, a candidate technology for manufacturing computer chips with gate lengths of 100 nm and smaller. The interferometer utilizes a spatially coherent spherical wavefront generated by pinhole spatial filtering of undulator radiation as described in this paper. It is a phase-shifting point diffraction interferometer [24] (PS/PDI), in which the optical system under test, in this case a 10× two-element, multilayer-coated Schwarzschild optic, forms an image of the pinhole "point source" at the mask plane. Inclusion of a transmission grating provides several diffracted orders, two of which are selected for use in the interferometer. Use of the grating improves efficiency and provides a linear phase-shifting capability through its lateral motion. Both orders interrogate the optical system, incur its aberrations (distorting the wavefronts), and come to focus at the mask plane. In normal operation, one order is allowed to pass through a large opening in the mask, preserving its distortions. The other order is spatially filtered by a second pinhole, providing a spherical reference wavefront for interferometric comparison at the EUV CCD detection plane. With a 10× reduction optical system, the second pinhole would nominally be 1 μm/10 = 100 nm in diameter. To determine the wavefront accuracy, defined as the rms departure from sphericity, a special null mask is used that spatially filters both orders, as shown in Fig. 11(a). Using two 100-nm pinholes, the resultant interference pattern is shown in Fig. 11(b). Analysis of the interference pattern yields the wavefront phase map shown in Fig. 11(c), revealing a departure from sphericity of 0.054 nm rms. This provides a measure of the wavefront accuracy [25] of the interferometer ($\lambda_{\mathrm{euv}}/250$) using spatially coherent undulator radiation and demonstrates a high degree of accuracy for testing nominally $\lambda_{\mathrm{euv}}/50$ optics. These tests were also performed using 80-nm pinholes yielding a wavefront accuracy of $\lambda_{\mathrm{euv}}/330$. More generally, this test provides a useful characterization for other experiments requiring spatially coherent spherical wavefronts at these very short wavelengths.

Another application that requires spatially coherent radiation is that of scanning microscopy, in which an optical system focuses a spherical wavefront to a spot size determined largely by wavelength and NA. At these short wavelengths, the focusing optic could be either a multilayer-coated Schwarzchild

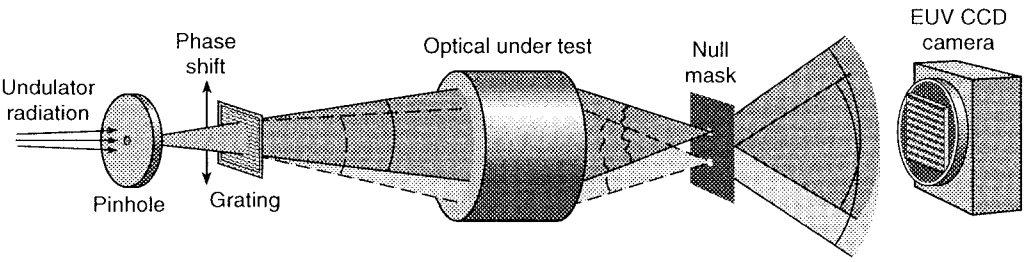

(a)

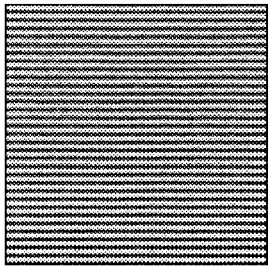

13.4 nm interference pattern

(b)

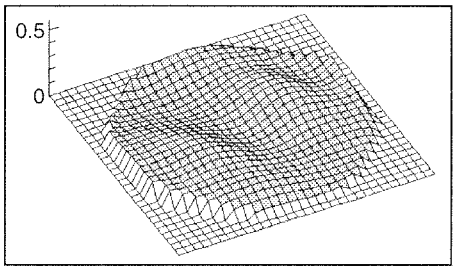

13.4 nm wavefront phase map

(c)

Fig. 11. (a) A schematic diagram of the PS/PDI that utilizes spatially filtered undulator radiation to measure aberrations in optical systems. An object plane pinhole, nominally 1 μm in diameter, is used to generate a spherical wave. The grating generates several orders, two of which are selected for use in the interferometer. The optic under test reimages the pinhole, in both selected orders, at the mask plane. In normal operation, the mask consists of one relatively large opening that passes the aberrated wavefront and one small pinhole, nominally 100 nm in diameter, to generate a spatially filtered spherical reference wave. For the wavefront accuracy measurements of interest here, a null mask with two 100-nm-diameter pinholes is used to generate two spherical wavefronts which interfere and are recorded by the CCD camera. (b) An interference pattern obtained at 13.4-nm wavelength utilizing two 100-nm-diameter pinholes. (c) The corresponding wavefront phase map which indicates an rms deviation from sphericity of $\lambda_{\rm euv}/250$, or 0.054 nm rms at 13.4-nm wavelength.

system or a Fresnel zone plate lens. In Fig. 7, a scanning photoemission microscope is indicated that receives photons through use of an insertable–retractable mirror (M3) in the beamline and also employs pinhole spatial filtering to generate the requisite spherical wavefront. This scanning microscope, which utilizes Ru–B_4C multilayer-coated Schwarzschild optics at 133 eV, has been developed by Cerrina *et al.* [35]–[37]. It is presently in use for the study of materials and materials chemistry of nanoelectronic structures at this beamline. Recent results are described by Lorusso *et al.* [36]. More recently, Kevan and his colleagues [38] have begun studies of nanostructure correlations in polymer thin films using speckle techniques and spatially coherent radiation available at this facility. Additional experiments, involving various interference effects and coherence characterization, are under way elsewhere [39]–[46].

VI. Conclusion

Broadly tunable coherent radiation is available at EUV and SXR wavelengths using spatially filtered undulator radiation. Experiments at the ALS, Berkeley, CA, verify the generation of broadly tunable high-wavefront-accuracy coherent power at the 10-μW level, with approximately 600 waves of temporal (longitudinal) coherence length. Extension to higher photon energies, approximately 1 keV, is straightforward using well-understood third-harmonic radiation. Further extension to spatially coherent radiation at a 1-Å wavelength should be available at sister facilities that operate at higher electron beam energies.

References

[1] D. T. Attwood, K. Halbach, and K.-J. Kim, "Tunable coherent X-ray," *Science*, vol. 228, p. 1265, 1985.
[2] A. M. Kondratenko and A. N. Skrinsky, "Use of radiation of electron storage rings in X-ray holography of objects," *Opt. Spektrosk. (USSR)*, vol. 42, p. 338, 1977; *Opt. Spectrosc.*, vol. 42, p. 189; *Opt. Soc. Amer.*, 1977.
[3] K.-J. Kim, "Characteristics of synchrotron radiation," in *Physics of Particle Accelerators*, M. Month and M. Dienes, Eds. New York: AIP, 1989, pp. 565–632.
[4] R. Coïsson, "Spatial coherence of synchrotron radiation," *Appl. Opt.*, vol. 34, p. 904, 1995.
[5] K. Halbach, "Permanent magnet undulators," *J. Phys.*, vol. 44, pp. C1–211, 1983.
[6] H. Winick, G. Brown, K. Halbach, and J. Harris, "Wiggler and undulator magnets," *Physics Today*, vol. 34, p. 50, May 1981.
[7] A. Hofmann, "Quasimonochromatic synchrotron radiation from undulators," *Nucl. Instrum. Methods*, vol. 152, p. 17, 1978; also "Theory of synchrotron radiation," SSRL ACD-Note, Stanford Univ., 1986.
[8] J. D. Jackson, "The impact of special relativity on theoretical physics," *Physics Today*, p. 34, May 1987.
[9] B. M. Kincaid, "A short-period helical wiggler as an improved source of synchrotron radiation," *J. Appl. Phys.*, vol. 48, p. 2684, 1977.
[10] M. R. Howells and B. M. Kincaid, "The properties of undulator radiation," in *New Directions in Research with Third-Generation Soft X-ray Synchrotron Radiation Sources*, A. Schlachter and F. Wuilleumier, Eds. Dordrecht, The Netherlands: Kluwer, 1994, p. 359.
[11] H. Winick, *Synchrotron Radiation Sources: A Primer*. Singapore: World Scientific, 1994.
[12] B. Goss Levi, "Many nations build the latest in synchrotron light sources," *Phys. Today*, p. 17, Apr. 1991.
[13] D. Attwood, *Soft X-rays and Extreme Ultraviolet Radiation: Principles and Applications*. Cambridge, U.K.: Cambridge Univ. Press, to be published.
[14] "An ALS handbook," Lawrence Berkeley National Laboratory, Berkeley CA, 1989, PUB-643, Rev. 2.
[15] A. Jackson, private communication, June 1998.
[16] H. Kitamura, "Future of synchrotron radiation," in *Kasokuki Kagaku (Accelerator Science)*. Tokyo: Ionics Publish, 1986, vol. 1, p. 45.

[17] M. Born and E. Wolf, *Principles of Optics*, 7th ed. Oxford, U.K.: Pergamon, 1999, ch. 10.
[18] J. Goodman, *Statistical Optics.* New York: Wiley, 1985.
[19] J. H. Underwood, unpublished.
[20] ——, "Spectrographs and monochromators using varied line space gratings," in *Methods of Vacuum Ultraviolet Spectroscopy*, J. A. R. Samson and D. L. Ederer, Eds. New York: Academic, 1998.
[21] R. Beguiristain, "Thermal distortion effects on beamline design for high flux synchrotron radiation," Ph.D. dissertation, Dept. Nuclear Engineering, Univ. California at Berkeley, Oct. 1997.
[22] M. Koike, R. Beguristain, J. H. Underwood, and T. Namioka, "A new optical design method and its application to an extreme ultraviolet varied line spacing plane grating monochromator," *Nucl. Instrum. Methods A*, vol. 347, p. 273, 1994.
[23] D. Attwood, G. Sommargren, R. Beguiristain, K. Nguyen, J. Bokor, N. Ceglio, K. Jackson, M. Koike, and J. H. Underwood, "Undulator radiation for at-wavelength interferometry of optics for extreme ultraviolet lithography," *Appl. Opt.*, vol. 32, p. 7022, 1993.
[24] H. Medecki, E. Tejnil, K. A. Goldberg, and J. Bokor, "A phase-shifting point diffraction interferometer," *Opt. Lett.*, vol. 21, p. 1526, Oct. 1996; H. Medecki, U.S. Patent 5 835 217, 1998.
[25] P. Naulleau, K. A. Goldberg, S. Lee, C. Chang, C. Bresloff, P. Batson, D. Attwood, and J. Bokor, "Characterization of the accuracy of EUV phase-shifting point diffraction interferometry," *SPIE*, vol. 3331, p. 114, 1998.
[26] K. A. Goldberg, P. Naulleau, C. Bresloff, P. Batson, P. Denham, S. H. Lee, C. Chang, E. Tejnil, D. Attwood, and J. Bokor, "Extreme ultraviolet interferometry: At-wavelength testing of optics for lithography," *J. Vac. Sci. Technol. B*, vol. 16, p. 3435, 1998.
[27] E. Tejnil, "Characterization of extreme ultraviolet imaging system," Ph.D. dissertation, Dept. Elect. Eng. and Computer Sci., Univ. California at Berkeley, 1997.
[28] K. A. Goldberg, "Extreme ultraviolet interferometry," Ph.D. dissertation, Dept. Physics, Univ. California at Berkeley, 1997.
[29] C. Montcalm, S. Bajt, P. B. Mirikami, E. Spiller, F. J. Weber, and J. A. Folta, "Multilayer reflective coatings for extreme ultraviolet lithography," *SPIE*, vol. 3331, p. 42, 1998.
[30] D. L. Windt and W. K. Waskiewicz, "Multilayer facilities required for extreme ultraviolet lithography," *J. Vac. Sci. Technol. B*, p. 3826, 1994.
[31] D. W. Sweeney, R. Hudyma, H. N. Chapman, and D. Shafer, "EUV optical design for a 100 nm CD imaging system," *SPIE*, vol. 3331, p. 2, 1998.
[32] E. Spiller, F. J. Weber, C. Montcalm, S. L. Baker, E. M. Gullikson, and J. H. Underwood, "Multilayer coating and tests of a 10X extreme ultraviolet lithography camera," *SPIE*, vol. 3331, p. 62, 1998; also see C. Montcalm, E. Spiller, J. A. Folta, and M. Wedowski, "Multilayer coating of 10X projection optics for extreme ultraviolet lithography," *SPIE*, vol. 3676, 1999.
[33] J. E. Bjorkholm, J. Bokor, R. Eichner, R. Freeman, J. Gregus, T. Jewell, W. Mansfield, A. MacDowell, E. Raab, W. Silfvast, L. Szeto, D. Tennant, W. Waskiewicz, D. White, D. Windt, O. Wood, and J. Bruning, "Reduction imaging at 14 nm using multilayer-coated optics printing features smaller than 0.1 μm," *J. Vac. Sci. Technol. B*, vol. 8, p. 1509, 1990.
[34] J. E. Goldsmith, P. K. Barr, K. W. Berger, L. J. Bernardez, G. F. Cardinale, J. R. Darnold, D. R. Folk, S. J. Haney, C. C. Henderson, K. L. Jefferson, K. D. Krenz, G. D. Kubiak, R. P. Nissen, D. J. O'Connell, Y. E. Parras, A. K. Ray-Chaudhuri, T. G. Smith, R. H. Stulen, D. A. Tichenor, A. A. Ver Berkmoes, and J. B. Wronosky, "Recent advances in the sandia EUV 10X microstepper," *SPIE*, vol. 3331, p. 11, 1998; also see J. Goldsmith *et al.*, "Sub-100 nm imaging with the EUV 10X microstepper," *SPIE*, vol. 3676, 1999.
[35] W. Ng, A. K. Ray-Chaudhuri, S. Liang, S. Singh, H. Solak, J. Welnak, F. Cerrina, G. Margaritondo, J. H. Underwood, J. B. Kortright, and R. C. C. Perera, "High resolution spectromicroscopy with MAXIMUM: Photoemission spectroscopy reaches 1,000 Å scale," *Nucl. Instrum. Methods A*, vol. 347, p. 422, 1994.
[36] G. F. Lorusso, H. Solak, F. Cerrina, J. H. Underwood, P. J. Batson, Y. Kim, Y. Cho, C. Kisielowski, J. Krueger, and R. E. Weber, "X-ray photoemission spectromicroscopy of GaN and AlGaN," in *MRS Proc.*, 1998, vol. 512, no. 393.
[37] H. H. Solak, G. F. Larusso, S. Singh-Gasson, and F. Cerrina, "*In situ* X-ray spectromicroscopic study of electromigration in patterned Al–Cu lines," *Appl. Phys. Lett.*, vol. 74, no. 22, 1999.
[38] S. Kevan, private communication.
[39] K. Fezaa, F. Comin, S. Mar.esini, R. Coïsson, and M. Belakhovsky, "X-ray interferometry at ESRF using two coherent beams from Fresnel mirrors," *J. X-Ray Sci. Technol.*, vol. 7, p. 12, 1997.
[40] D. L. Abernathy, G. Grübel, S. Bauer, I. McNulty, G. B. Stephenson, S. G. J. Mochrie, A. R. Sandy, N. Mulders, and M. Sutton, "Small-angle X-ray scattering using coherent undulator radiation at ESRF," *J. Synchr. Rad.*, vol. 5, p. 37, 1988.
[41] P. Müller-Buchsbaum, T. Thurn-Albrecht, G. Meier, M. Stam, E. W. Fischer, B. Stark, B. Stühn, D. L. Abernathy, and G. Grübel, "Observation of speckle patterns by coherent X-ray scattering from thin polymer films," *ESRF Newsletter*, Sept. 1998.
[42] A. Snigirev, I. Snigireva, V. Kohn, S. Kuznetsov, and I. Schelokov, "On the possibilities of X-ray phase contrast microimaging by coherent high-energy synchrotron radiation," *Rev. Sci. Instrum.*, vol. 66, p. 5486, 1995.
[43] Z. H. Hu, P. A. Thomas, A. Snigirev, I. Snigireva, A. Souvorov, P. G. R. Smith, G. W. Ross, and S. Teats, "Phase-mapping of periodically domain-inverted $LiNbO_3$ with coherent X-rays," *Nature*, vol. 392, p. 690, 1998.
[44] Y. Takayama, R. Z. Tai, T. Hatano, T. Miyahara, W. Okamoto, and Y. Kagoshima, "Measurement of the coherence of synchrotron radiation," *J. Synchr. Rad.*, vol. 5, p. 456, 1998.
[45] J. I. Espeso, P. Cloetens, J. Baruchel, J. Härtwig, T. Mairs, J. C. Baisci, G. Marot, M. Salomé-Pateyron, and M. Schlenker, "Conserving the coherence and uniformity of third-generation synchrotron radiation beams," *J. Synchr. Rad.*, vol. 5, p. 1243, 1998.
[46] F. Livet, F. Bley, A. Létoublon, J. P. Simon, and J. F. Bérar, "Coherent small-angle scattering on a bending-magnet beamline at the ESRF," *J. Synchr. Rad.*, vol. 5, p. 1337, 1998.

David T. Attwood received the B.S. degree in engineering science from Hofstra University, Hempstead, NY, in 1963, the M.S. degree from Northwestern University in Evanston, IL, in 1965, and the D.Engr.Sci. degree in applied physics from New York University, New York, in 1972.

He worked in the Laser Fusion Program at Lawrence Livermore National Laboratory, Livermore, CA, from 1972 to 1983. Since 1983, he has been at the Lawrence Berkeley National Laboratory, Berkeley, CA, where he is Director of the Center for X-ray Optics. He has been teaching at the University of California at Berkeley since 1986, where he is Professor in Residence in Electrical Engineering and Computer Science.

Patrick Naulleau received the B.S. and M.S. degrees in electrical engineering from the Rochester Institute of Technology, Rochester, NY, in 1991 and 1993, respectively, and the Ph.D. degree in electrical engineering from the University of Michigan at Ann Arbor in 1997. His Ph.D. research concentrated on coherence and speckle techniques for imaging through highly scattering media and optical fibers.

Since 1997, he has been at Lawrence Berkeley National Laboratory, Berkeley, CA, where he works at the Center for X-ray Optics in the area of extreme ultraviolet interferometry.

Kenneth A. Goldberg received the A.B. degrees in physics and applied mathematics and the M.A. and Ph.D. degrees in physics from the University of California at Berkeley in 1992, 1994, and 1997, respectively.

He now works at the Center for X-ray Optics at Lawrence Berkeley National Laboratory, Berkeley, CA, developing novel measurement techniques for extreme ultraviolet optical systems. His scientific interests include interferometry, short-wavelength optics, and lithography.

Edita Tejnil received the B.S., M.S., and Ph.D. degrees from the Electrical Engineering and Computer Sciences Department, University of California at Berkeley, in 1992, 1994, and 1997, respectively. Her thesis work focused on high-accuracy wavefront metrology of reflective optics for extreme ultraviolet lithography applications.

She is currently with the Intel Corporation, working on advanced lithography and photomask solutions for future integrated circuit technologies.

Chang Chang received the B.S. degree in electrical engineering from National Taiwan University, Taipei, Taiwan, in 1996, and the M.E. degree from the School of Electrical Engineering, Cornell University, Ithaca, NY, in 1997. He is now working toward the Ph.D. degree in the Department of Electrical Engineering and Computer Science, University of California at Berkeley.

He is currently working on the coherence properties of undulator radiation at Lawrence Berkeley National Laboratory, Berkeley, CA.

Raul Beguiristain received the B.S. degree in nuclear engineering/physics from the University of Maryland, College Park, in 1987 and the Ph.D. degree in applied science and technology and nuclear engineering from the University of California at Berkeley in 1997.

He worked in the Center for X-ray Optics at Lawrence Berkeley National Laboratory, Berkeley, CA, as a Staff Scientist from 1997 to 1998. He is currently working as a Scientist at Adelpi Technology, Inc., Palo Alto, CA.

Phillip Batson received the A.A. degree in mechanical engineering technology from City College, San Francisco, CA, in 1962 and the A.A. degree in electronics engineering from Merritt College, Oakland, CA, in 1975.

He is a Mechanical Engineering Group Leader at Lawrence Berkeley National Laboratory, Berkeley, CA. He worked at the Hilac and Super Hilac at Lawrence Berkeley National Laboratory from 1962 to 1984. Since 1984, he has been with Lawrence Berkeley National Laboratory's Center for X-ray Optics.

Jeffrey Bokor (S'75–M'90–SM'95) received the B.S. degree in electrical engineering from the Massachusetts Institute of Technology, Cambridge, in 1975 and the M.S. and Ph.D. degrees in electrical engineering from Stanford University, Stanford, CA, in 1976 and 1980, respectively.

From 1980 to 1993, he was at AT&T Bell Laboratories where he did research on novel sources of ultraviolet and soft X-ray coherent radiation, advanced lithography, picosecond optoelectronics, semiconductor physics, surface physics, MOS device physics, and integrated circuit process technology. He held management positions as head of the Laser Science Research Department at Bell Labs, Holmdel, NJ, from 1987 to 1990, and head of the ULSI Technology Research Department at Bell Labs, Murray Hill, NJ. He joined the Department of Electrical Engineering and Computer Sciences at the University of California at Berkeley in 1993 as a Full Professor, with a joint appointment in the Center for X-ray Optics at Lawrence Berkeley National Laboratory, Berkeley, CA. His current research activities include nanoelectronics, deep submicro MOSFET device physics, extreme ultraviolet projection lithography, and ultrafast phenomena in electronic materials.

Eric M. Gullikson received the B.S. degree in physics from the University of Hawaii, in 1977 and the Ph.D. degree in physics from the University of California at San Diego in 1984.

He was performed postdoctoral research at Bell Laboratories from 1984 to 1987. Since 1987, he has been at Lawrence Berkeley National Laboratory, Berkeley, CA, where he is a Staff Scientist in the Center for X-ray Optics.

Masato Koike received the B.Education degree in science from Wakayama University, Wakayama, Japan, in 1974, the M.S. degree from Tokyo University of Education, Tokyo, Japan, in 1976, and the D.Engr. degree in applied physics from Osaka City University, Osaka, Japan, in 1979.

He worked in the Optical Devices Department, Shimadzu Corporation, in Kyoto, Japan, from 1979 to 1989. He worked at Lawrence Berkeley National Laboratory, Berkeley, CA, where he was Staff Scientist at the Center for X-ray Optics from 1989 to 1997. He is now at the Japan Atomic Energy Research Institute, Kyoto, Japan, where he is a Senior Scientist in the Advanced Photon Research Center.

Hector Medecki received the Diploma Engineer, Aeronautics, and Electronics degrees from the Superior Aeronautical School, Argentine Air Force University, Argentina, in 1954.

He worked at Lawrence Livermore National Laboratory, Livermore, CA, from 1985 to 1993, working on projects such as target fabrication for laser fusion and X-ray lasers. He came to the Center for X-ray Optics at Lawrence Berkeley National Laboratory, Berkeley, CA in 1993 to work on soft X-ray microscopy and extreme ultraviolet interferometry.

James H. Underwood received the B.Sc. and Ph.D. degrees in physics from the University of Leicester, U.K., in 1959 and 1964, respectively.

In 1963, he joined the NASA-Goddard Space Flight Center as an NSF-NRC Post-Doctoral Fellow, and continued to work on NASA spacecraft projects for the next 20 years, designing X-ray and extreme ultraviolet (EUV) telescopes for sounding rockets and spacecraft projects such as the Orbiting Solar Observatory and Skylab. In 1983, he joined the Center for X-ray Optics at Lawrence Berkeley National Laboratory, Berkeley, CA, where he has specialized in the development of X-ray and EUV reflecting multilayers and the design of monochomators and beamlines at the Advanced Light Source.